Department of Energy & Environmental Systems, North Carolina A&T State University AST 885-005

Orographic Precipitating Systems

Dr. Yuh-Lang Lin, ylin@cat.edu; https://mesolab.org
North Carolina A&T State University
(Ref.: *Mesoscale Dynamics*, Y.-L. Lin, Cambridge, 2007)

Chapter 17 Dynamics of Orographic Precipitation

(Based on Ch. 11 of Mesoscale Dynamics (Lin 2007)) (Classical equation editor: $c_p \neq f(k)$)

17.1 Orographic influence on climatological distribution of precipitation

- Climatological distribution of precipitation is significantly influenced by the mountains.

  Example 1: Figure 11.1 shows the mean annual precipitation for 1971-90 over Western Europe.

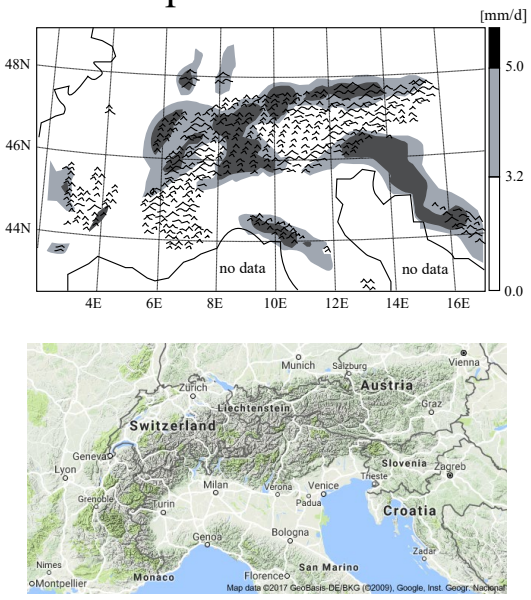

Fig. 11.1: Mean annual precipitation over land for the period 1971-1990 over Western Europe. The dark (light) shaded areas denote averaged daily precipitation higher than 5.0 mm d^{-1} (in between 3.2 and 5.0 mm d^{-1}). Terrain higher than 800 m is approximately denoted by mountain

symbol. (Adapted after Frei and Schär 1998)

- Example 2 & 3: Annual rainfall distributions in South America and Taiwan (Fig. 11.2 of Lin 2007)

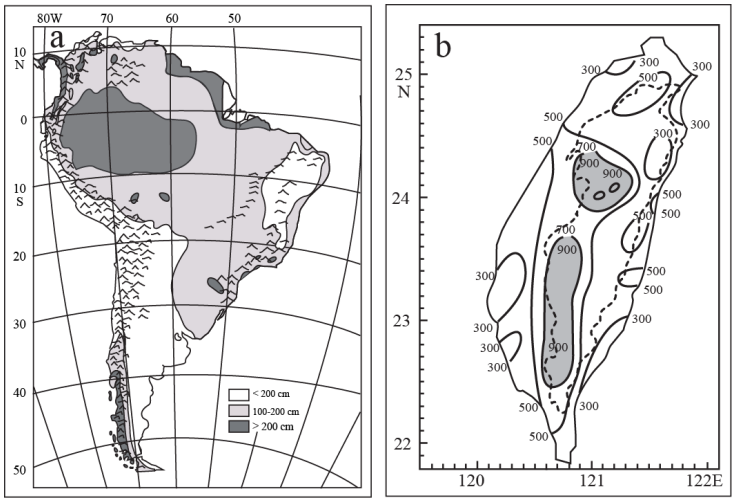

Fig. 11.2: (a) Annually averaged rainfall distribution over the Andes in South America. (Adapted after Espenshade et al. 1990). The dark (light) shaded areas denote annual precipitation higher than 200 cm (in between 100 – 200 cm). The terrain higher than 900 m is approximately denoted by the mountain symbol. (b) Total rainfall distribution during the TAMEX (10 May-27 June 1987) from 808 daily rainfall stations in Taiwan. The prevailing wind is the monsoonal flow from the southwest. Rainfall contours (thick) start at 300 mm with 200-mm intervals. The dashed contour denotes the terrain height of 1 km. (Adapted after Yeh and Chen 1998) [from Lin 2007]

  - Figure 11.2a reveals that the annual rainfall distribution over the Andes in South America has rainfall maxima located on the eastern slope in northern Andes (to the north of 30°S) under the prevailing easterly and westerly winds, respectively, and on the western slope in southern Andes.
  - Figure 11.2b indicates the rainfall was produced mainly from the lifting and blocking of the prevailing wind from the southwesterly monsoonal flow and the modification on mesoscale convective systems and Mei-Yu fronts moving from the west toward the western slopes of Taiwan's Central Mountain Range (CMR).

- The maximum rainfall over a small hill is often located over the mountain peak or downwind slope due to a shorter advection time required for an air parcel to pass over or go around the hill, compared to the formation time for orographic clouds and precipitation.

Figure 11.3a shows how maximum rainfall areas coincide with the terrain in a plot of rainfall amounts and distribution observed on March 28, 1953 over Wales, UK.

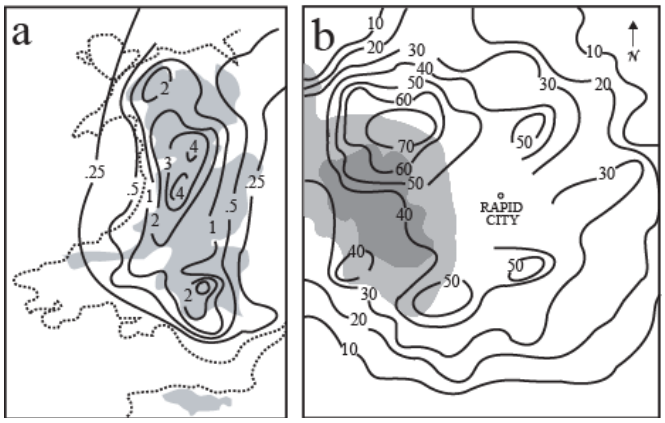

Fig. 11.3: Rainfall maxima located over the peak or leeside of small hills: (a) Rainfall observed over Wales, UK on 28 March 1953. Rainfall contours are in inches. Shaded areas denote the terrain higher than 150 m (Adapted after Sawyer 1956); and (b) Radar echo frequency of rain-showers for all year in the southwesterly wind cases over four summers of 1967-70 in Black Hills, South Dakota. Shaded areas denote the terrain height contours (1372 and 1676 m). (Adapted after Kuo and Orville 1973)

- The precipitation distribution over meso-γ mountains or small hills, however, does not necessarily coincide with the terrain contours. For example, Fig. 11.3b shows the echo frequency associated with summertime rain-showers observed over the Black Hills of South Dakota. There are double maxima in echo frequency: one located over the northeastern and the other over the southeastern section of the Black Hills.

➢ The intensity, duration and distribution of orographic precipitation are mainly determined by the following factors (Sawyer 1956):

- *Large-scale environment* which determines the characteristics of the airflow upstream of the mountain, such as wind speed and direction, stability, and relative humidity;
- *Dynamics of the air motion* over and around the mountain, which determines the location and layer of orographic clouds and precipitation; and

- *Cloud microphysical processes* which determine the characteristics of the cloud and precipitation systems and formation time in the vicinity of the mountain.

Under the orographically-modified upstream airflow associated with the large-scale environment, the interaction between the dynamical processes and cloud microphysical processes is extremely complicated, thus making quantitative forecasting of orographic precipitation very difficult and one of the most challenging problems in numerical weather prediction.

14.2 Orographic modification of pre-existing disturbances

- Mountains usually modify, and often amplify, rather than create precipitation (Smith 2006).
- A prevailing wind or pre-existing weather system influences the orographic precipitation by:

  (1) Providing larger-scale upstream conditions, such as wind speed and direction, humidity and stability;

  (2) Generating additional forcing through dynamical processes due to its interaction with the topography.

  The additional forcing includes pressure gradient force associated with orographically-modified flow circulations, convergence or divergence, and the latent heat release; and

  (3) Affecting the microphysical processes in orographic cloud formation by providing the characteristics of hydrometeors and stability, and through its interaction with the topography.

- Common synoptic and mesoscale environments conducive to heavy orographic precipitation are often very complicated:

  (1) A mid- and upper-tropospheric shortwave trough just upstream from the flood location, which is propagating towards the high-pressure ridge axis;

(2) A massive middle-upper tropospheric westward-tilted ridge of high pressure;
(3) A very strong upslope, low-level jet (LLJ) from the east or southeast and a southward-propagating shallow cold front;
(4) A very high θ_e (equivalent potential temperature) associated with the LLJ;
(5) Conditional instability associated with the airflow upstream of the mountain;
(6) Weak mid- and upper-tropospheric steering currents.

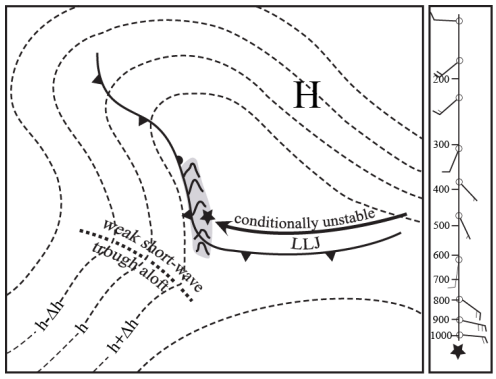

Fig. 11.4: Schematic of the synoptic and mesoscale conditions conducive to heavy orographic rainfall, based on the observations of the 1972 Rapid City, South Dakota flood, 1977 Big Thompson Canyon, Colorado flood, the 1997 Fort Collins, Colorado flood, and the 1995 Madison County, Virginia flood. Displayed are the surface synoptic features (fronts and high), threat region (star), mountains (shaded), low-level jet (LLJ), 500-hPa height field (dashed lines) and short-wave trough (heavy dotted curve), and typical wind profile above the threat region (right panel). (Adapted after Pontrelli et al. 1999; Lin 2007)

➢ Figure 11.5 shows a schematic for the synoptic and mesoscale environments conducive to Alpine heavy orographic rain.

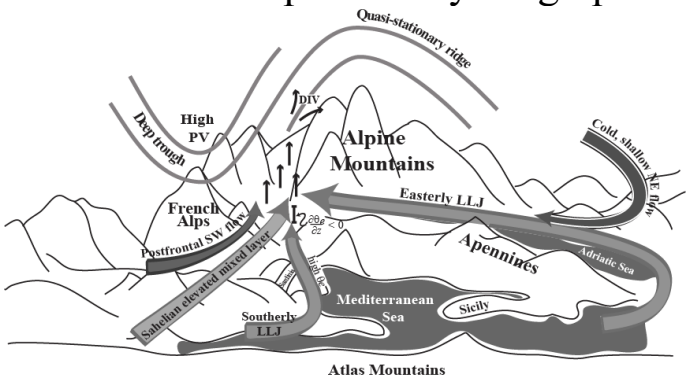

Fig. 11.5: A schematic for the synoptic and mesoscale environments conducive to heavy orographic rain in the Alps. (Lin 2007, Adapted after Lin 2005)

➢ Figure 11.9 shows a conceptual model of orographic rain triggered by the LLJ associated with a cold front and a land-falling extratropical cyclone over the California Coastal Range and Sierra Nevada mountains.

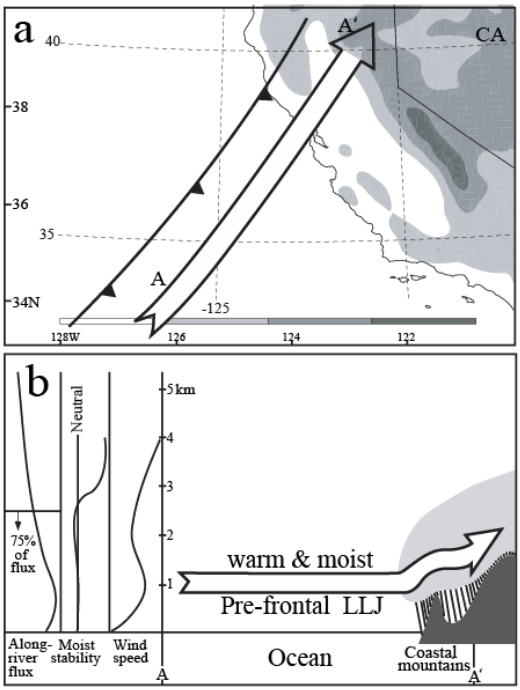

Fig. 11.9: A conceptual model of orographic rain triggered by the LLJ associated with a cold front and a land-falling extratropical cyclone over a perpendicular mesoscale mountain range. This is based on the observations over the California Coastal Range and Sierra Nevada mountains (shaded with 3 height levels). (a) Plan view schematic showing the relative positions of an LLJ and trailing polar cold front. (b) Schematic along the pre-frontal LLJ (i.e., along AA' in (a)). The vertical structures of wind speed, moist static stability, and along-atmospheric-river moisture flux far upstream of the mountain ranges are depicted. Schematics of orographic clouds and precipitation are also shown. (Adapted after Ralph et al. 2005)

- The prefrontal LLJ is narrow, warm and almost moist neutral, which is very effective in transporting the water vapor toward the California coast.

- The narrow, almost moist neutral region of strong water vapor transport is also referred to as *atmospheric river*.

- Orographic rain associated with the passage of a tropical depression over the mountains in Kyushu island

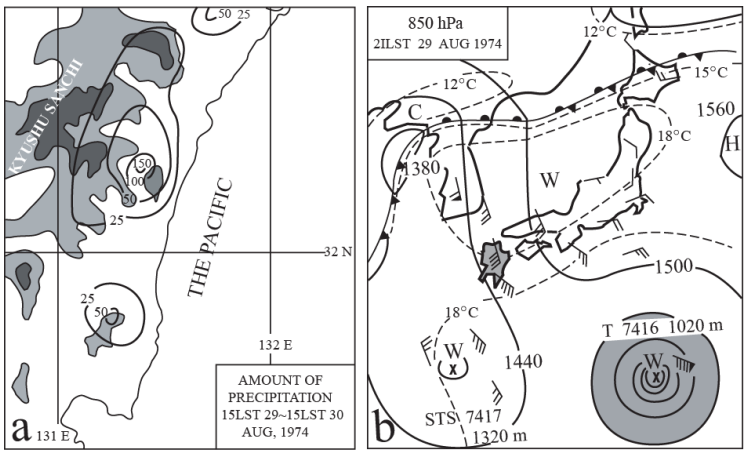

Fig. 11.10: Orographic rain associated with the passage of a tropical depression over the mountains in Kyushu island (both the island and the tropical depression are shaded in (b)). (a) Daily amount of precipitation (in mm) in the vicinity of the Kyushu Sanchi during the event (terrain higher than 500 m and 1000 m are dark and light shaded, respectively). (b) Synoptic situation at 12UTC (21LST) 29 August 1974 depicted by 850 hPa map around Japan Islands (bold curves). The solid and dashed lines represent geopotential height and temperature contours, respectively. (After Sakakibara 1979)

- Similar phenomena also occur in heavy orographic rain events in other parts of the world, such as over the southwest concave region of the CMR of Taiwan (Fig. 11.11).

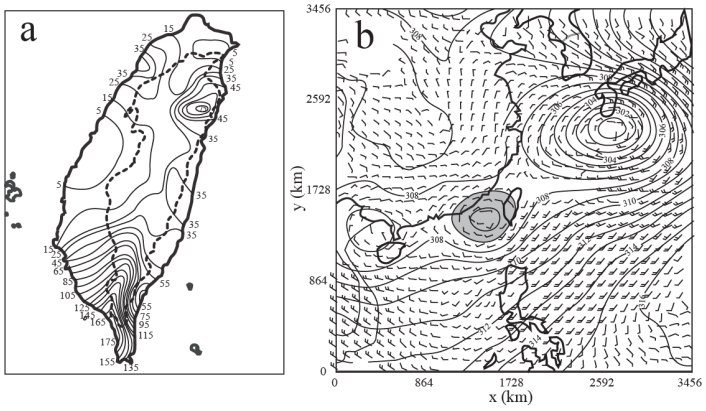

Fig. 11.11: Heavy orographic rainfall produced by the passage of a tropical storm (shaded in (b)) over the Central Mountain Range (CMR), Taiwan. The dashed contour denotes the terrain height of 1 km. (a) Accumulated rainfall (in mm) over Taiwan from 0000 UTC 6 August to 0000 UTC 7 August 1999. (b) NCEP reanalysis data over East Asia valid at 1200 UTC 6 August 1999 for vector wind (1 full bar = 5 ms^{-1}) and geopotential height at 700 hPa. (Adapted after Lin et al. 2001)

➢ *Common ingredients of orographic precipitation*

Based on the above discussion, there are some common synoptic and mesoscale features for producing heavy orographic rainfall associated with the passage of a weather system, such as

- Steep mountain
- LLJ, high θ_e
- High CAPE
- Quasi-stationary synoptic system (e.g. a typhoon, a high pressure ridge, or a stationary front).

These common features may be explained by taking a common ingredient approach as follows.

➢ The total precipitation (P) is determined by the average rainfall rate (R) and the duration (D),

$$P = RD \,. \tag{11.2.1}$$

The rainfall rate can then be determined by the *precipitation efficiency*, E, and the *vertical moisture flux*, wq_v,

$$R = E(\rho / \rho_w)\,(wq_v)\,, \tag{11.2.2}$$

where ρ_w is the liquid water density, ρ and q_v are the lower moist layer average air density and the water vapor mixing ratio. Substituting (11.2.2) into (11.2.1) leads to

$$P = E\ (\rho / \rho_w)(wq_v)\ D\,. \tag{11.2.3}$$

The duration of heavy rainfall may be estimated by

$$D = L_s / c_s\,, \tag{11.2.4}$$

where L_s and c_s are the horizontal scale of the convective system and its propagation speed in the direction of the system movement, respectively.

Combining (11.2.3) and (11.2.4) leads to

$$P = E(\rho / \rho_w)(wq_v)(L_s / c_s) \quad . \tag{11.2.5}$$

Equation (11.2.5) implies that when the value of any combined factors on the right-hand side is large, there is a potential for heavy rainfall.

Based on (11.2.5), a set of essential ingredients for flash floods over a flat surface have been proposed (Doswell et al. 1998).

For flow over a mountain range, the low-level upward vertical motion is induced by either orography or the environment (e.g., upper-tropospheric divergence),

$$w = w_{oro} + w_{env} \tag{11.2.6}$$

The orographically-forced upward vertical motion may be roughly estimated by the lower boundary condition for flow over mountains, which is done by extending (5.1.10) to three dimensions:

$$w_{oro} = \frac{Dh}{Dt} \approx \boldsymbol{V}_H \cdot \nabla h \quad , \tag{11.2.7}$$

where $h(x, y)$ is the mountain height as a function of x and y, and $\boldsymbol{V}_H$ is the low-level horizontal wind velocity.

Similar forms of (11.2.7) have been proposed in different studies (e.g., Alpert 1986; Sinclair 1994).

The environmentally-forced upward vertical motion (w_{env}) can be determined by the transient synoptic setting, such as the divergence associated with an approaching trough or conditional instability. Combining (11.2.5) – (11.2.7) gives

$$P = E(\rho / \rho_w)\ \left(\boldsymbol{V_H} \cdot \nabla h + w_{env}\right)\ q_v\ (L_s / c_s)\ . \qquad (11.2.8)$$

Besides the ingredients included in (11.2.8), as discussed in subsection 11.2.3, a conditionally or potentially unstable airstream may also help trigger deep convection by parcel or layer lifting forced by orography.

Based on these arguments, the extremely heavy orographic rainfall requires significant contributions from any combination of the following common ingredients:

(1) high precipitation efficiency of the incoming airstream (large E), a low-level jet (large $|\boldsymbol{V}_H|$),
(2) steep orography (large ∇h),
(3) a low-level jet (LLJ, large $\boldsymbol{V}_H$),
(4) a confluent flow field (large $\boldsymbol{V}_H \cdot \nabla h$),
(5) strong synoptically forced upward vertical motion (large w_{env}),
(6) a moist unstable low-level flow (large w_{env}),
(7) a high moisture flow upstream (large q_v),
(8) presence of a large, pre-existing convective system (large L_s), and slow or impeded movement of the convective system (small c_s).

Further reading: Lin et al. (2001), Lin (2007, sec. 11.2.4).

- Note that the vertical velocity is normally not a linear superposition of *environmentally* and *orographically forced vertical motions*, since they interact with each other nonlinearly.

  For example, w_{env} associated with the release of conditional instability requires a finite-amplitude orographically-induced upward motion (w_{oro}).

  However, the partitioning of w into w_{oro} and w_{env} helps recognize the dynamics and the prediction of the precipitation distribution directly initiated by the orographic lifting, instead of the prediction of the amount of orographic precipitation.

Part of the two-dimensional form of (11.2.8), $U(\partial h/\partial x)q$ (where $\boldsymbol{V_H}$ reduces to U for a uniform flow), can be used as an index for the prediction of upslope heavy orographic precipitation if the negative values are neglected (Alpert 1986).

The index has been applied to some of the historical events of heavy orographic precipitation discussed earlier, and can help to provide additionally valuable information for the prediction of the occurrence of upstream heavy orographic precipitation events.

In fact, the three-dimensional form, $(\boldsymbol{V_H} \cdot \nabla h) q_v$, representing the *general moisture flux*, can be used to help predict the precipitation distribution (e.g., Witcraft et al. 2005), which is especially useful for climatological and hydrological applications, which represents the *orographic moisture flux*.

14.3 Formation and enhancement mechanisms

- Formation and enhancement mechanisms of orographic precipitation are extremely complicated and are highly dependent on the dynamical and thermodynamic conditions of the upstream airflow, interactions between different layers of clouds, interactions between dynamical and cloud microphysical processes, and mountain geometry.

- In the past, several major formation and enhancement mechanisms have been proposed:

  (1) stable ascent
  (2) release of moist instabilities
  (3) effects of mountain geometry
  (4) combined thermal and orographic forcing,
  (5) seeder-feeder mechanism
  (6) interaction of dynamical and microphysical processes

These mechanisms are sketched in Fig. 11.12 and will be discussed in the following.

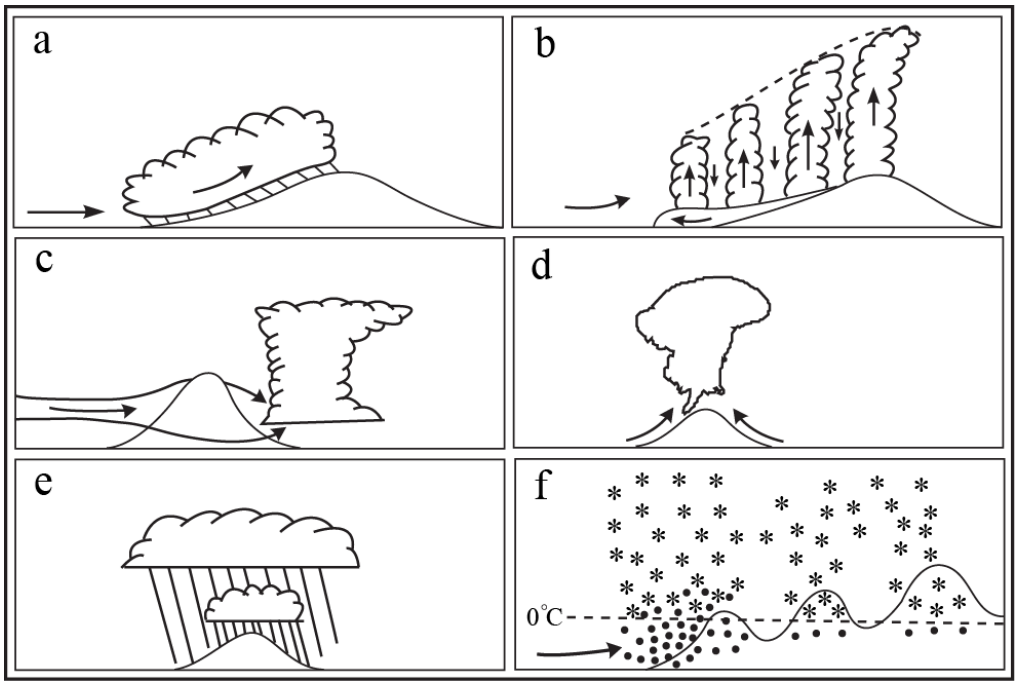

Fig. 11.12: Conceptual models of the formation and enhancement mechanisms of orographic precipitation: (a) stable ascent, (b) release of moist instabilities, (c) effects of mountain geometry, (d) combined thermal and orographic forcing, (e) seeder-feeder mechanism, and (f) interaction of dynamical and thermodynamic processes. (Lin 2007, adapted after Smith 1979; Banta 1990; Houze 1993; Medina and Houze 2003)

14.4 Control parameters and moist flow regimes

14.4.1 Control parameters

- Based on the above discussion of synoptic and mesoscale environments and common ingredients for heavy orographic precipitation, the formation and propagation of an orographic precipitation system in a two-dimensional, approximately moist stable flow appear to be controlled by a number of flow and orographic parameters, such as

- basic wind speed (U),
- saturated moist Brunt-Vaisala frequency (N_m, as defined in (7.3.12)),
- mountain height (h),
- mountain width scale (a),
- earth rotation (f), and
- vertical wind shear (U_z).

➢ In order to thoroughly understand the complicated dynamics of orographic precipitation, the theoretical approach and/or a systematic approach for performing idealized nonlinear numerical simulations are required.

➢ Ideally, it is desirable to choose a set of independent, nondimensional control parameters to avoid varying too many dimensional control parameters. The use of control parameters will also make the theoretical results more general.

➢ Practically, it is very difficult to take into account all of the dimensional parameters controlling the orographic precipitation formation and propagation. However, this can still be partially accomplished by working on a subset of the dimensional control parameters.

➢ For example, one may choose to start with a subset of the above-mentioned dimensional control parameter, (U, N_m, h, a). A set of independent, nondimensional control parameters can then be determined by the *Buckingham-*Π *theorem*.

➢ The Buckingham-Π theorem states that the number of nondimensional combinations (parameters) involved in a mathematical model is equal to the difference between the number of original quantities and the number of fundamental dimensional units, such as time, mass, and length.

- Applying the Buckingham-Π theorem to the four dimensional parameters listed above, i.e. U, N_m, h, and a, leads to two independent nondimensional parameters because there are only the two primary quantities, i.e. length and time, involved in the system.

- One may choose the *moist Froude number*, $F_m = U / N_m h$, as a nondimensional control parameter. Similar to the dry Froude number ($F = U / Nh$), the reciprocal of the moist Froude number is also called the *nondimensional mountain height*, which represents the strength of nonlinearity.

- That is, larger (smaller) F_m represents a more linear (nonlinear) flow.

- A second nondimensional control parameter is the mountain slope or height-width aspect ratio, defined as h / a, or the nondimensional mountain width, $N_m a / U$.

- Both h / a and $N_m a / U$ measure the non-hydrostatic effects.

- The flow becomes more nonhydrostatic when h / a increases. Similar to dry airflow over mountains (Ch. 5), for $N_m a / U >> 1$, the flow reaches hydrostatic balance.

- On the other hand, the non-hydrostatic effects cannot be ignored if this criterion is not met.

- Analogous to dry flow, among F_m, h / a, and $N_m a / U$, only two of them can be chosen for the nondimensional control parameter space since they are not independent of each other.

- For a conditionally unstable flow over mountains, one may define the moist Froude number as $F_w = U / N_w h$ (Chen and Lin 2005a), where N_w is the unsaturated Brunt-Vaisala frequency defined as:

$$N_w^2 = \frac{g}{\theta_v}\frac{\partial \theta_v}{\partial z} . \qquad (11.4.1)$$

  In the above equation, θ_v is the virtual potential temperature for moist, but unsaturated air. In this situation, CAPE also becomes a factor in determining the flow responses.

- For a potentially unstable flow, the criterion $\partial \theta_e / \partial z < 0$ needs to be considered. When the mountain geometry is considered, the horizontal width aspect ratio a / b is applied, where a and b are the horizontal scales in the direction parallel and perpendicular to the basic wind, respectively.

- For a flow over a meso-α scale or larger scale mountain, then the rotational effects need to be considered. In this case, the Rossby number, U / fa, or the Burger number, nh / fa, is a natural choice for an additional nondimensional control parameter.

14.4.2 Moist flow regimes
(a) Two-dimensional flow regimes

- Figure 11.22 demonstrates the dependency of the flow on the moist Froude number with $F_m = 0.67$, 1.33, and 2.0. In the numerical experiments, the flow is designed to be nearly moist-neutral with 98% relative humidity.
- The F_m is varied by changing the basic wind speed for 10, 20, and 30 ms^{-1}.

- For $F_m = 0.67$, a shallow orographic cloud forms over the windward slope (Fig. 11.22a). A well-defined wave cloud forms over the lee slope, while subsidence exists immediately above the crest.

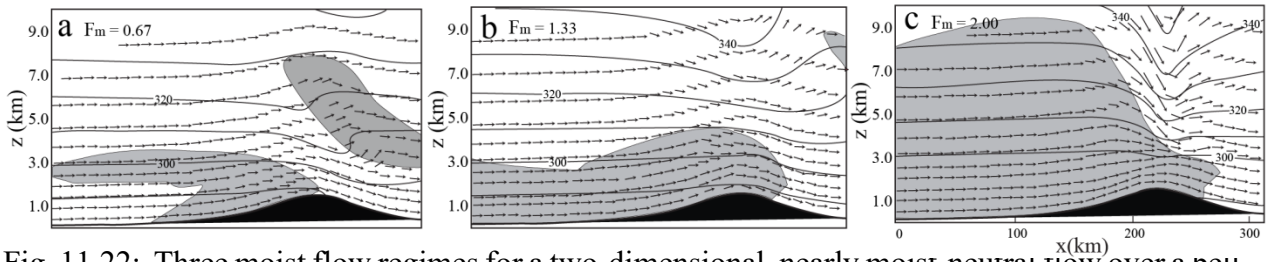

Fig. 11.22: Three moist flow regimes for a two-dimensional, nearly moist-neutral flow over a bell-shaped mountain with F_m=: (a) 0.67, (b) 1.33, and (c) 2.00. F_m is the saturated moist Froude number defined as $U / N_m h$. The flow and precipitation are averaged from numerically simulated fields for 6 to 12 h. The orographic and flow parameters are: h = 1.5 km, a = 50 km (half-width of the mountain), N_m = 0.01 s^{-1}, and U = 10, 20, and 30 ms^{-1}. The corresponding $N_m a / U$ are 50, 25, and 16.67, respectively. Displayed are the potential temperature (solid), wind vectors, and total precipitation hydrometer (rain, snow and graupel) mixing ratio higher than 0.04 g kg^{-1} (shaded). (Lin 2007, adapted after Colle 2004)

- For $F_m = 1.33$, the orographic cloud over the windward slope extends over the mountain peak and farther upstream, mainly due to the deepening of the upward motion to 3 km over the upslope and the downstream advection of the hydrometeors (Fig. 11.22b).

- For $F_m = 2.0$, the area of ascending motion deepens over the lower upslope to above 9 km, resulting in a deep orographic snow cloud and more precipitation upstream of the mountain (Fig. 11.22c). Since $N_m a / U$ (=50, 25, and 16.67) is much larger than 1, the flow is approximately in hydrostatic balance. The hydrostatic vertical wavelength for the case of $F_m = 2.0$ is roughly equal to 18.84 km (Fig. 11.22c), which is much larger than 6.28 km for the case of $F_m = 0.67$.

- This contributes to the deeper orographic clouds in the larger F_m cases. The vertical velocity near the mountain surface is approximately proportional to $w' \approx U\partial h / \partial x$, which gives a much higher vertical velocity for the $F_m = 2.0$ case, compared to that for the $F_m = 0.67$ case. Thus, a higher F_m may trigger more active microphysical processes and more precipitation.

➢ The behavior of a conditionally unstable flow over mountains is very different from that of a moist stable flow over mountains.

By varying the unsaturated moist Froude number (F_w) associated with a two-dimensional conditionally unstable flow over a mountain ridge, three moist flow regimes may be identified:

(I) upstream propagating convective system,
(II) stationary convective system, and
(III) both stationary and downstream propagating systems.

Figure 11.23 illustrates the time evolution of rainwater content at the height of 1 km above the surface and the horizontal wind speed for $F_w = 0.208$, 0.354, and 0.833, which correspond to $U = 2.5$, 4.25, and 10 ms^{-1}, respectively.

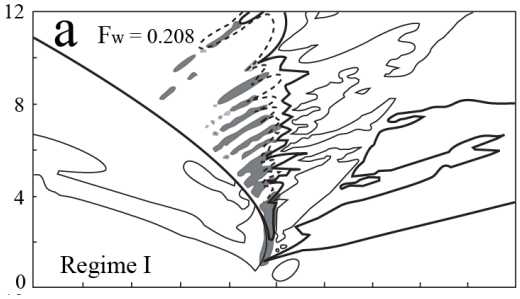

Fig. 11.23: Three moist flow regimes for a conditionally unstable airflow over a mesoscale mountain, based on the unsaturated, moist Froude number F_w =: (a) 0.208 (Regime I), (b) 0.354 (Regime II), and (c) 0.833 (Regime III). F_w is defined in (11.4.1). The corresponding basic flow speeds are $U = 2.5$, 4.25, and 10 ms^{-1}, respectively. Displayed are the time evolutions of surface wind (dashed, thin-solid, and heavy-solid contours for -5, 0, and 5 ms^{-1}, respectively) and rainwater (shaded for $q_r \geq 0.5$ g kg^{-1}) at 1 km height above the surface, as simulated by a mesoscale model (ARPS, see Xue et al. 2001). (Lin 2007, adapted after Chu and Lin 2000)

- For the case of $F_w = 0.208$ (Regime I), the density current generated by the orographically triggered convective clouds propagates upstream of the mountain. The embedded individual convective cells are generated at the gust front of the density current and then propagate downstream once they form. However, the convective system propagates upstream along with the density current (Fig. 11.23a).

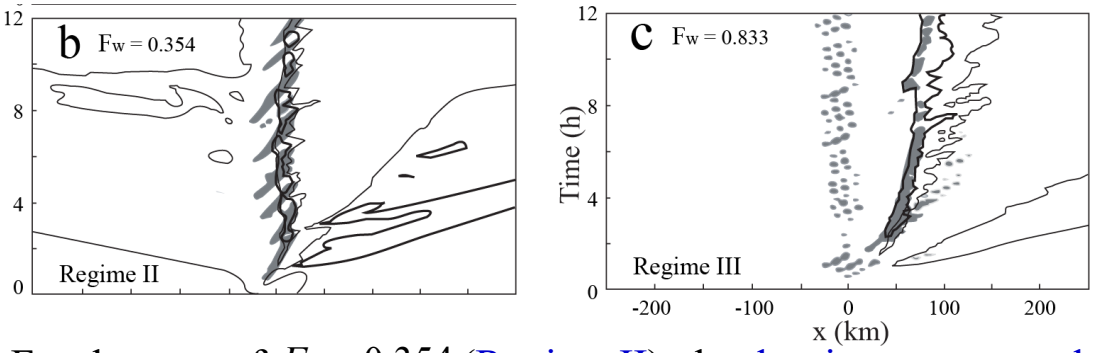

- For the case of $F_w = 0.354$ (Regime II), the density current, and thus the convective system, becomes quasi-stationary in the vicinity of the mountain peak (Fig. 11.23b). Both propagating and growing modes of convective cells found in multicell storms (Ch. 8) are present in this flow regime. The convective system is maintained by a balance between the orographic forcing and the density current forcing.

- For the case of $F_w = 0.833$ (Regime III), the density current propagates downstream and two convective systems exist: the quasi-stationary system and the downstream propagating system (Fig. 11.23c). For the stationary convective system, the cell generation is similar to that of regime II, but weaker in strength.

- Figure 11.24 shows a schematic of the four moist flow regimes generated by different sets of F_w and CAPE.

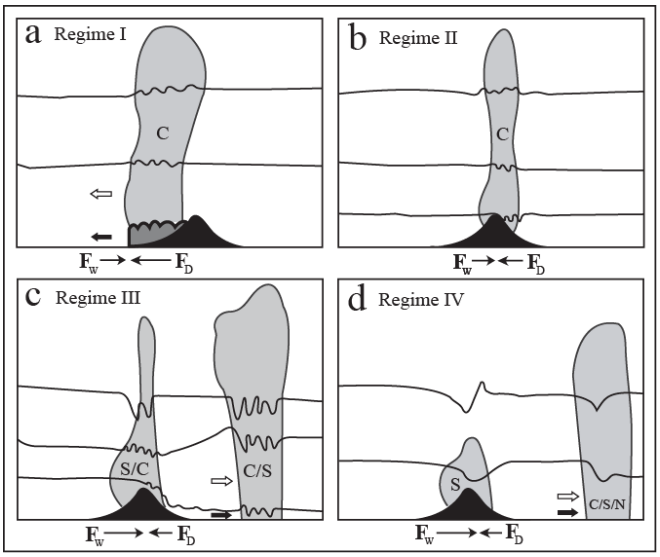

Fig. 11.24: Schematic of the four moist flow regimes for a conditionally unstable airflow over a mesoscale mountain for (F_w , *CAPE*) =: (a) (small, large), (b) (small, small), (c) (large, large), and (d) (large, small). Flow regimes in (a) – (c) are identical to regimes I-III shown in Figs. 11.23a-c. Flow regime IV is characterized by an orographic stratiform precipitation system over the mountain and a downstream-propagating cloud system. Below each panel, $\mathbf{F}_w$ and $\mathbf{F}_D$ denote the forcing associated with the basic flow and density current/cold pool, respectively. Isentropes and cloud boundaries are denoted by solid and dashed curves, respectively. Symbols C, S, and N denote convective, stratiform, and no-cloud types, respectively. Outline (filled) arrow denotes the propagation direction of the precipitation system (density current). (Lin 2007, adapted after Chen and Lin 2005a)

- The flow regimes of Figs. 11.24a-c are identical to Regimes I-III shown in Figs. 11.23a-c, except that the cloud system in the vicinity of the mountain peak is a mixture of convective clouds and stratiform clouds (Fig. 11.23c).

- Flow regime IV is characterized by an orographic stratiform precipitation system over the mountain and a downstream-propagating cloud system.

  The long-lasting orographic stratiform precipitation system is due to the shorter advection time compared with cloud growth time. Strong

upward propagating gravity waves are generated by the mountain and the downstream propagating cloud system, as revealed by the isentropes.

- The formation and propagation of different flow regimes may be interpreted from the competition between the forcing associated with the basic flow and the forcing associated with the density current or cold pool. The latter is strongly linked to the strength of the convective system and thus related to the magnitude of the CAPE.

- An extreme case in the (F_w, CAPE) parameter space is a moist neutral flow over a mesoscale mountain ridge.

  Three flow subregimes are found for:
  (1) lower mountains, a saturated flow can be maintained everywhere given sufficient initial cloud water;
  (2) higher mountains, the upstream atmosphere is maintained in a saturated state and transitions to an unsaturated downslope flow on the lee side, which has characteristics associated with downslope windstorms; and
  (3) mountains of intermediate height, an upstream-propagating disturbance develops, which tends to de-saturate the atmosphere above the mountain (Miglietta and Rotunno 2005).

(b) Three-dimensional flow regimes

- For flow over a three-dimensional isolated mountain, as expected, flow behaves differently from that over a two-dimensional mountain ridge.

- Numerical studies have demonstrated that the reduction of effective static stability of a southerly moist flow by latent heating may go through the regime transition from flow-around a higher mountain ridge to flow-over lower mountain ridge (Buzzi et al. 1998; Ferretti et al. 2000), which is consistent with the idea of F_m as a moist flow control parameter.

- For a nearly moist-neutral (RH = 98%) flow over a three-dimensional isolated mountain, three flow regimes, similar to those discussed in the two-dimensional moist flow regimes (Subsection 11.4.2(b)) are also identified (Miglietta and Buzzi 2001).
- The Froude number also controls the propagation of nocturnal cloud bands formed by the downslope drainage flow and the basic easterly trade wind (e.g., Smolarkiewicz et al. 1988).
- Regimes I-III for a conditionally unstable flow over a two-dimensional mountain, as described above, are also found in flow over three-dimensional, isolated mountain (Chen and Lin 2005b).
- In addition, a relatively stronger basic flow, such as a low-level jet, is able to produce a quasi-stationary mesoscale convective system and maximum rainfall on the windward slope (i.e., upslope precipitation), instead of on the mountain peak or on the lee slope, which is more consistent with observations.
- The change in preferred upslope precipitation accumulation is due to the fact that the three-dimensional isolated mountain allows the upstream airflow to split and flow around it.

  Regimes I and II discussed above have been reproduced by simulating a conditionally unstable flow represented by an upstream condition of MAP IOP-2B over the Alpine mountains (Stein 2004).

Appendix:

- A quick review of ***conditional instability*** and ***potential (convective) instability*** (Ch. 7 of Lin 2007)
  - Conditional Instability

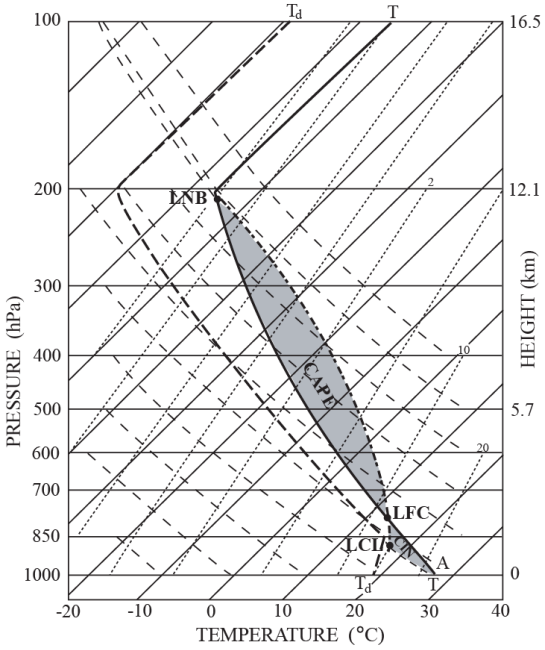

Fig. 7.5: Example of an idealized sounding with conditional instability displayed on a *skew-T log-p* thermodynamic diagram. The isotherms, saturation mixing ratio, and dry sadiabat are denoted by slanted solid, dotted, and dashed curves. The environmental temperature (T) and dew point profile (T_d) are denoted by thick solid and dashed curves, respectively. The lifting condensation level (LCL), level of free convection (LFC), and level of neutral buoyancy (LNB) for the air parcel originated at A are denoted in the figure. The convective available potential energy (CAPE) is the area enclosed by the temperature profile and the moist adiabat (thick dot-dashed curve) in between LFC and LNB, while the convective inhibition (CIN) is the area enclosed by the temperature profile and the dry adiabat (below LCL) and the temperature profile and the moist adiabat (in between LCL and LFC).

- The criterion for conditional instability may also be determined via the vertical gradient of the *saturation equivalent potential temperature* (θ_e^*), which is defined as the equivalent potential temperature of a hypothetically saturated atmosphere. This hypothetical atmosphere has the same thermal structure as the actual atmosphere.
- In other words, the θ_e^* can be defined as the equivalent potential temperature the air parcel would have if it were saturated at the same pressure and temperature,

$$\theta_e^* = \theta \exp(Lq_{vs} / c_p T). \qquad (7.3.24)$$

The criterion for conditional instability can also be determined via the vertical gradient of the *saturation equivalent potential temperature* (θ_e^*) which is defined as the equivalent potential temperature of a hypothetically saturated atmosphere at the initial level. This hypothetical atmosphere has been set to mimic the thermal structure of the actual atmosphere. In other words, θ_e^* can be defined as the equivalent potential temperature that the air parcel would have if it were saturated initially at the same pressure and temperature, and can be calculated by

$$\theta_e^* = \theta e^{Lq_{vs}/c_pT}. \tag{7.3.17}$$

In order to derive the criterion for conditional instability, we consider an air parcel lifted from $z_o - \delta z$ to z_o. At $z_o - \delta z$, the air parcel is assumed to have the same potential temperature as that of the environment, $\bar{\theta} - (\partial\bar{\theta}/\partial z)\eta$, where $\bar{\theta}$ is the potential temperature of the environmental air at z_o, and $\eta = \delta z$ is the vertical displacement. The potential temperature of the air parcel experiences a change of $\delta\theta$ when it is lifted from $z_o - \eta$ to z_o, i.e. $[\bar{\theta} - (\partial\bar{\theta}/\partial z)\eta] + \delta\theta$. Thus, the buoyancy of the air parcel at z_o is

$$b = g\left(\frac{\theta - \bar{\theta}}{\bar{\theta}}\right) = -\frac{g}{\bar{\theta}}\frac{\partial\bar{\theta}}{\partial z}\eta + g\frac{\delta\theta}{\bar{\theta}}. \tag{7.3.18}$$

Substituting the heating rate ($\dot{q}$) from latent heat release, $\dot{q} = -L(Dq_{vs}/Dt)$, into (2.2.5) gives

$$\frac{\delta\theta}{\bar{\theta}} \approx -\delta\left(\frac{Lq_{vs}}{c_pT}\right) \approx -\frac{\partial}{\partial z}\left(\frac{Lq_{vs}}{c_pT}\right)\eta. \tag{7.3.19}$$

Substituting (7.3.19) into (7.3.18) and using the definition of θ_e^* leads to

$$b \approx -\left(\frac{g}{\bar{\theta}_e^*}\frac{\partial\bar{\theta}_e^*}{\partial z}\right)\eta. \tag{7.3.20}$$

Substituting the above equation into (7.3.2) for a moist atmosphere, gives us

$$\frac{D^2\eta}{Dt^2}+\left(\frac{g}{\bar{\theta}_e^*}\frac{\partial\bar{\theta}_e^*}{\partial z}\right)\eta=0. \qquad (7.3.21)$$

Therefore, *the conditional stability criterion for a saturated layer of air becomes*

$$\frac{\partial\bar{\theta}_e^*}{\partial z}\begin{cases}>0 & \text{conditionally stable}\\ =0 & \text{conditionally neutral}\\ <0 & \text{conditionally unstable}\end{cases} \qquad (7.3.22)$$

Note that in addition to $\partial\bar{\theta}_e^*/\partial z<0$, the release of conditional instability requires the air parcel to be lifted above its LFC. This requirement is not included in the above derivation (e.g. Sherwood 2000; Schultz et al. 2000). Parcel theory also neglects the effects of mass continuity and pressure perturbation (Xu 1986), as also known from dry static instability.

➢ As shown above, it can be derived

$$\frac{D^2\eta}{Dt^2}+\left(\frac{g}{\bar{\theta}_e^*}\frac{\partial\bar{\theta}_e^*}{\partial z}\right)\eta=0$$

Therefore, the conditional stability criterion for a saturated layer of air becomes

$$\frac{\partial\bar{\theta}_e^*}{\partial z}\begin{cases}>0 & \text{conditionally stable}\\ =0 & \text{conditionally neutral}\\ <0 & \text{conditionally unstable}\end{cases} \qquad (7.3.29)$$

➢ Potential (Convective) Instability (PI)

Potential instability is also referred to as *convective instability* in the literature, and describes a condition in which an atmospheric layer becomes unstable statically after lifting.

- It is based on layer theory.

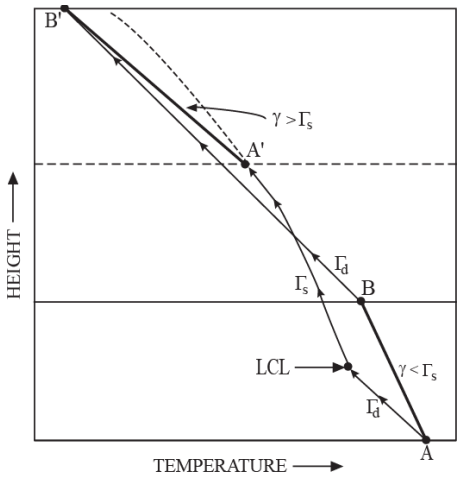

Fig. 7.6: Illustration of potential (convective) instability by lifting an initially absolutely stable layer AB with $\partial\overline{\theta}_e/\partial z < 0$. The top of the layer (B) follows a dry adiabat to saturation at B', while the bottom of the layer becomes saturated earlier (at LCL) and then follows moist adiabat to A'. The lapse rate of the final saturated layer (A'B') is greater than the moist adiabat, thus is unstable. (Adapted after Darkow 1986)

- Note that in the same environment CI may occur, but not PI. For example, Fig. 7.7 shows θ_e^* and θ_e surfaces on a cross section from Dauphin, Manitoba (YDN) to Minneapolis-St. Paul (MSP) forecast by Rapid Update Cycle (RUC) valid at 0000 UTC 3 January 1998. Although the air above the frontal surface is conditionally unstable since $\partial\theta_e^*/\partial z < 0$ (Fig. 7.7a), it is potentially stable since $\partial\theta_e/\partial z > 0$ (Fig. 7.7b).

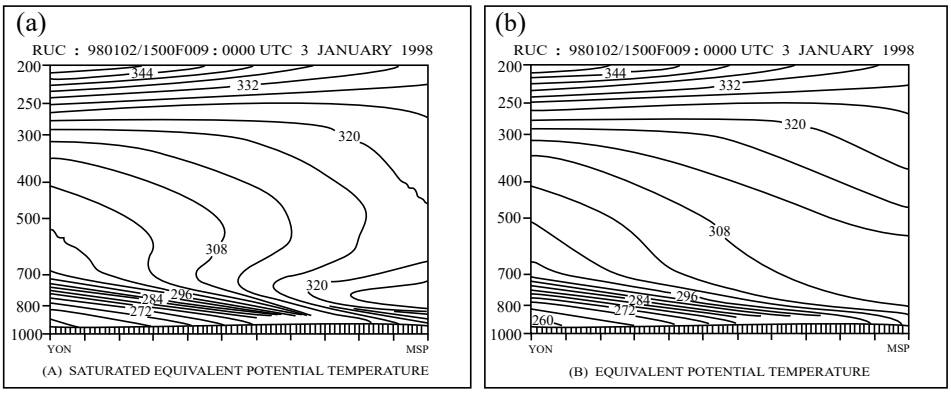

Fig. 7.7: (a) Saturation equivalent potential temperature ($\overline{\theta}_e^*$) and (b) equivalent potential temperature ($\overline{\theta}_e$) fields on the cross section from Dauphin, Manitoba (YDN) to Minneapolis-St. Paul, Minnesota (MSP), as predicted by the Rapid Update Cycle for 9-h forecast valid for 0000 UTC 3 January 1998. Note that above the surface cold front, the air is conditionally unstable ($\partial\overline{\theta}_e^*/\partial z < 0$), but is potentially stable ($\partial\overline{\theta}_e/\partial z > 0$). (Adapted after Schultz and Schumacher 1999)